≪Review Paper≫ Applied Science and Convergence Technology Vol.23 No.2, March 2014, pp.72~82
http://dx.doi.org/10.5757/ASCT.2014.23.2.72

Recent Development in the Rate Performance of $Li_4Ti_5O_{12}$

Chunfu Lin[a], Yuelong Xin[b], Fuquan Cheng[b], Man On Lai[a], Henghui Zhou[b]*, and Li Lu[a]*

[a]*Department of Mechanical Engineering, National University of Singapore, Singapore 117576, Singapore*
[b]*College of Chemistry and Molecular Engineering, Peking University, Beijing 100871, PR China*

(Received March 21, 2014, Revised March 31, 2014, Accepted March 31, 2014)

Lithium-ion batteries (LIBs) have become popular electrochemical devices. Due to the unique advantages of LIBs in terms of high operating voltage, high energy density, low self-discharge, and absence of memory effects, their application range, which was primarily restricted to portable electronic devices, is now being extended to high-power applications, such as electric vehicles (EVs) and hybrid electrical vehicles (HEVs). Among various anode materials, $Li_4Ti_5O_{12}$ (LTO) is believed to be a promising anode material for high-power LIBs due to its advantages of high working potential and outstanding cyclic stability. However, the rate performance of LTO is limited by its intrinsically low electronic conductivity and poor Li^+ ion diffusion coefficient. This review highlights the recent progress in improving the rate performance of LTO through doping, compositing, and nanostructuring strategies.

Keywords : Lithium-ion battery, Lithium titanate, Rate performance, Doping, Compositing, Nanotructuring

I. Introduction

Due to energy and environmental concerns, intensive attention has been paid to the development of lithium ion batteries (LIBs) with high power density for large format energy storage system applications, such as electric vehicles (EVs) and hybrid electrical vehicles (HEVs) [1]. At present, the market penetration of EVs/HEVs is severely limited by the low rate performance of LIBs. Graphite has been proven to be a reliable anode material in commercial LIBs for portable electronic devices [2]. However, its rate capability is limited. When the operation current density is large, it suffers from severe polarization, causing metallic lithium to deposit on its surface [3,4]. Safety problems will emerge if this process is repeated many times, due to the growth of lithium dendrites. Therefore, to develop LIBs with high rate performance for EVs/HEVs, it is necessary to explore anodes with good rate performance and safety.

$Li_4Ti_5O_{12}$ (LTO), with a theoretical capacity of 175 mAh g^{-1}, is considered a promising substitute for carbon-based anodes in LIBs. It has a high working potential of about 1.55 V (all the potentials in this review refer to Li/Li^+) [5,6], thereby avoiding the growth of lithium dendrites. It has a spinel structure with a $Fd\bar{3}m$ space group, as illustrated in Fig. 1 [7]. All O^{2-} ions are located at 32e sites, forming a cubic closest packed structure. All Ti^{4+} ions and 25% of Li^+ ions are disordered, occupying the octahedral 16d sites. As a

* [E-mail] luli@nus.edu.sg
hhzhou@pku.edu.cn

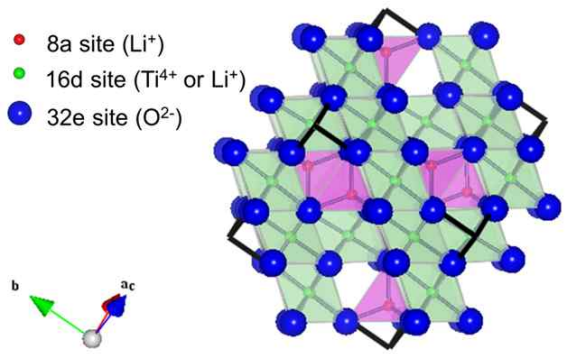

Figure 1. Schematic representation of the LTO structure.

result, the molar ratio of Ti^{4+} and Li^+ ions is 5:1. The remaining octahedral cation sites (16c sites) are vacant. The remaining Li^+ ions fill the tetrahedral 8a sites. For one formula unit of $Li_4Ti_5O_{12}$, during the lithiation process, three Li^+ ions in 8a sites and three external Li^+ ions cooperatively move to 16c sites, leading to the formation of $Li_7Ti_5O_{12}$ with a rock salt structure; during the delithiation process, the process is reversed and $Li_4Ti_5O_{12}$ is regenerated. In this reversible reaction, the robust three-dimensional framework $[LiTi_5]^{16d}[O_{12}]^{32e}$ is not changed and its volume change is negligible (<0.1%) [8], greatly benefiting its reversibility and cyclic stability.

However, LTO suffers from intrinsically low electronic conductivity ($<1\times10^{-13}$ S cm^{-1}) and a poor Li^+ diffusion coefficient ($\sim10^{-15}$ cm^2 s^{-1}), significantly limiting its rate performance [9,10]. During the lithiation/delithiation process, Li^+ ions intercalate/deintercalate into/from the LTO lattice accompanied by electrons. Obviously, the conduction of LTO depends on the electronic conductivity and the Li^+ ion diffusion coefficient in LTO particles, electrical conduction between the particles, and particle size. With higher electronic conductivity and a larger Li^+ ion diffusion coefficient in the particles, better electrical conduction takes place between the particles, and smaller particle size benefits the conduction and thus the rate performance of LTO. Intensive studies have been conducted to improve the rate performance through doping, compositing, and nanostructuring strategies. In this report, recent progress in the improvement of the rate performance is reviewed. The doping, compositing, and nanostructuring strategies are compared and discussed in detail.

II. Doping Strategy

Doping with alien ions in Li^+, Ti^{4+} or O^{2-} sites of LTO crystals can effectively modify the electronic conductivity and/or Li^+ ion diffusion coefficient in LTO particles, although this strategy cannot increase the electrical conduction between particles. The effective dopants include Ca^{2+} [11], Mg^{2+} [12], Al^{3+} [13,14], Mo^{6+} [15], Nb^{5+} [16,17], Zn^{2+} [18], Ru^{4+} [19], Zr^{4+} [20], W^{6+} [21], La^{3+} [22], V^{5+} [23], Ta^{5+} [24], Cr^{3+} [25], Ni^{2+} [26], Cu^{2+} [27], Cl^- [28], and Br^- [29]. By enhancing the electronic conductivity and/or Li^+ ion diffusion coefficient via doping, the rate performance of LTO can be improved.

1. Doping in Li^+ site

Zhang et al. prepared $Li_{4-x}Ca_xTi_5O_{12}$ ($0\leq x\leq0.2$) through a solid-state reaction method in an air atmosphere [11]. The Ca^{2+} doping enhanced both the electronic conductivity and the Li^+ ion diffusion coefficient in the particles. Among all the Ca^{2+} doped LTO samples, $Li_{3.9}Ca_{0.1}Ti_5O_{12}$ showed the highest electronic conductivity and Li^+ ion diffusion coefficient. As a result, it exhibited outstanding rate performance with a reversible capacity of 139 mAh g^{-1} at 10 C in a potential range of 1.0~2.5 V. Chen et al. synthesized $Li_{4-x}Mg_xTi_5O_{12}$ ($0\leq x\leq1$) through a solid-state reaction method in an H_2/He atmosphere [12]. The substitution of Mg^{2+} ions for Li^+ ions led to a reduction of an equivalent number of Ti^{4+} ions from Ti^{4+} to Ti^{3+} based on charge balance, and thus a ultra-high electronic conductivity of 10^{-2} S cm^{-1}. Consequently,

the rate performance of LTO was improved. Zhao et al. fabricated $Li_{4-x}Al_xTi_5O_{12}$ ($0 \leq x \leq 0.2$) through a solid-state reaction method in an argon atmosphere [13]. Due to the Al^{3+} doping, the electronic conductivity in the particles was increased through the generation of mixing Ti^{4+}/Ti^{3+}. However, the Li^+ ion diffusion coefficient was decreased due to the blockage of Al^{3+} ions in 8a sites of the spinel crystal structure. The former effect overwhelmed the latter, leading to improved rate performance of $Li_{4-x}Al_xTi_5O_{12}$. The optimized sample, $Li_{3.8}Al_{0.2}Ti_5O_{12}$, had a capacity of 130 mAh g^{-1} at 3 C in 1.0～2.3 V.

2. Doping in Ti^{4+} site

Zhang et al. synthesized $Li_4Ti_{4.95}Mo_{0.05}O_{12}$ through a solid-state reaction method in a H_2/Ar atmosphere [15]. The substitution of Mo^{6+} ions for Ti^{4+} ions enhanced the electronic conductivity of LTO through the generation of mixing Ti^{4+}/Ti^{3+}. As a result, $Li_4Ti_{4.95}Mo_{0.05}O_{12}$ showed outstanding rate performance with a reversible capacity of 117 mAh g^{-1} at 10 C and 94 mAh g^{-1} at 30 C in 1.0～3.0 V. Tian et al. prepared $Li_4Ti_{4.95}Nb_{0.05}O_{12}$ through a citric acid-assistant sol-gel method [16]. $Li_4Ti_{4.95}Nb_{0.05}O_{12}$ delivered a large capacity of 120 mAh g^{-1} at 10 C in 0～2.5 V since both the electronic conductivity and the Li^+ ion diffusion coefficient of LTO were improved by Nb^{5+} doping. Yi et al. fabricated microscale $Li_4Ti_{5-x}Zn_xO_{12}$ ($0 \leq x \leq 0.2$) particles through a solid-state reaction [18]. $Li_4Ti_{4.9}Zn_{0.1}O_{12}$ exhibited a Li^+ ion diffusion coefficient of 1.38×10^{-12} cm^2 s^{-1}, which was 185 times larger than that of pristine LTO. The capacity of $Li_4Ti_{4.8}Zn_{0.2}O_{12}$ was 186 mAh g^{-1} at 5 C in 0～2.5 V. Lin et al. prepared $Li_4Ti_{5-x}Al_xO_{12}$ (x=0, 0.05) materials through a facile sol-gel process [14]. Both the electronic conductivity and the Li^+ ion diffusion coefficient in the particles were improved by the substitution of Al^{3+} ions for Ti^{4+} ions. $Li_4Ti_{4.95}Al_{0.05}O_{12}$ consequently showed good rate performance with a capacity of 116 mAh g^{-1} at 5 C in 1.0～2.5 V and a capacity of 185 mAh g^{-1} at 5 C in 0～2.5 V. Wang et al. synthesized $Li_4Ti_{5-x}Ru_xO_{12}$ through a reverse micro-emulsion method with subsequent calcination [19]. Due to the larger ion size of Ru^{4+} than Ti^{4+}, the lattice parameter in $Li_4Ti_{5-x}Ru_xO_{12}$ is larger than that of pristine LTO. This enlargement benefited the insertion and extraction of Li^+ ions. Therefore, $Li_4Ti_{4.95}Ru_{0.05}O_{12}$ presented excellent rate performance with a large capacity of 131 mAh g^{-1} at 60 C in 0.01～2.5 V. Yi et al. fabricated $Li_4Ti_{5-x}Zr_xO_{12}$ ($0 \leq x \leq 0.25$) materials through a solid-state reaction method [20]. Both the electronic conductivity and Li^+ ion diffusion coefficient in the particles were enhanced by Zr^{4+} doping, leading to improvement of the rate performance. In 0～3.0 V, $Li_4Ti_{4.9}Zr_{0.1}O_{12}$ delivered a capacity of 155 mAh g^{-1}. Zhang et al. prepared $Li_4Ti_{4.95}W_{0.05}O_{12}$ through a solid-state reaction method [21]. The substitution of W^{6+} ions for Ti^{4+} ions increased the electronic conductivity in the particles through the generation of mixing Ti^{4+}/Ti^{3+}. Consequently, $Li_4Ti_{4.95}W_{0.05}O_{12}$ exhibited advanced rate performance with a reversible capacity of 131 mAh g^{-1} at 10 C and 119 mAh g^{-1} at 20 C in 1.0～3.0 V. Yi et al. fabricated micro-sized $Li_4Ti_{5-x}La_xO_{12}$ ($0 \leq x \leq 0.2$) particles through a facile solid-state reaction method in an air atmosphere [22]. Both the electronic conductivity and the Li^+ ion diffusion coefficient in the particles were improved due to the La^{3+} doping. The optimized sample, $Li_4Ti_{4.95}La_{0.05}O_{12}$, displayed the highest electronic conductivity and Li^+ ion diffusion coefficient, and thereupon showed the best rate performance. It delivered a reversible capacity of 201 mAh g^{-1} at 5 C in 0～2.5 V. Yu et al. prepared $Li_4Ti_{4.9}V_{0.1}O_{12}$ powders through a simple solid-state reaction method in an inert atmosphere [23]. The electronic conductivity of $Li_4Ti_{4.9}V_{0.1}O_{12}$ was as high as 2.9×10^{-1} S cm^{-1}, which was ascribed to the transformation of some Ti^{3+} ions from Ti^{4+} ions induced by V^{5+} doping. Furthermore, $Li_4Ti_{4.9}V_{0.1}O_{12}$ exhibited a Li^+ ion diffusion coefficient of 6.5×10^{-13} cm^2 s^{-1}, which was 240 times larger than

that of pristine LTO. As a result, $Li_4Ti_{4.9}V_{0.1}O_{12}$ showed advanced rate performance with a reversible capacity of 117 mAh g^{-1} at 5 C in 1.0～2.5 V. Hu et al. synthesized $Li_4Ti_{4.95}Ta_{0.05}O_{12}$ through a solid-state reaction method [24]. Ta^{5+} doping not only increased the electronic conductivity in the particles through the generation of mixing Ti^{4+}/Ti^{3+}, but also enhanced the Li^+ ion diffusion coefficient in the particles. Consequently, $Li_4Ti_{4.95}Ta_{0.05}O_{12}$ exhibited outstanding rate performance with a reversible capacity of 116 mAh g^{-1} at 10 C and 91 mAh g^{-1} at 30 C in 1.0～3.0 V. Tian et al. fabricated $Li_4Ti_{4.95}Nb_{0.05}O_{12}$ through a sol-gel method [17]. Compared with the pristine LTO, $Li_4Ti_{4.95}Nb_{0.05}O_{12}$ exhibited higher electronic conductivity and a larger Li^+ ion diffusion coefficient. Therefore, $Li_4Ti_{4.95}Nb_{0.05}O_{12}$ showed excellent rate performance with a reversible capacity of 135 mAh g^{-1} at 10 C, 127 mAh g^{-1} at 20 C, and 80 mAh g^{-1} at 40 C in 1.0～2.5 V.

3. Doping in Li^+ and Ti^{4+} sites

Sun et al. prepared $Li_{(4-x)/3}Cr_xTi_{(5-2x)/3}O_{12}$ ($0 \leq x \leq 1$) compounds through a solid-state reaction method [25]. In Cr^{3+} doped LTO, every two Ti^{4+} ions and every Li^+ ion are replaced by three Cr^{3+} ions. Both the electronic conductivity and Li^+ ion diffusion coefficient in the particles were improved by Cr^{3+} doping. The optimized compound, $LiCrTiO_4$, had an improved rate performance with a capacity of 88 mAh g^{-1} at 2 C in 1.2～3.0 V. Our group fabricated $Li_{4-2x}Ni_{3x}Ti_{5-x}O_{12}$ ($0 \leq x \leq 0.25$) through a solid-state reaction method [26]. In this type of Ni^{2+} doped LTO, every two Li^+ ions and every Ti^{4+} ion are substituted by three Ni^{2+} ions. The best electronic conductivity of Ni^{2+} doped LTO was at least one order of magnitude higher than that of the pristine LTO due to the introduction of Ni^{2+} ions with free 3d electrons. As a result, Ni^{2+} doped samples had favorable rate performance, with $Li_{3.9}Ni_{0.15}Ti_{4.95}O_{12}$ showing the best performance. At 5 C, it has a high capacity of 72 mAh g^{-1}, which is 1.2 times larger than that of pristine LTO. Our group also synthesized $Li_{4-2x}Cu_{3x}Ti_{5-x}O_{12}$ using the same solid-state reaction method [27]. Due to the Cu^{2+} doping, the electronic conductivity and Li^+ diffusion coefficient of the particles were respectively improved by at least two orders of magnitude and four times, leading to advanced rate performance of $Li_{4-2x}Cu_{3x}Ti_{5-x}O_{12}$, as shown in Fig. 2. At 10 C, $Li_{3.8}Cu_{0.3}Ti_{4.9}O_{12}$ showed a capacity of 78 mAh g^{-1} in 1.0～2.5 V.

4. Doping in O^{2-} site

Huang et al. fabricated $Li_4Ti_5O_{12-x}Cl_x$ ($0 \leq x \leq 0.3$) through a high-temperature solid-state reaction

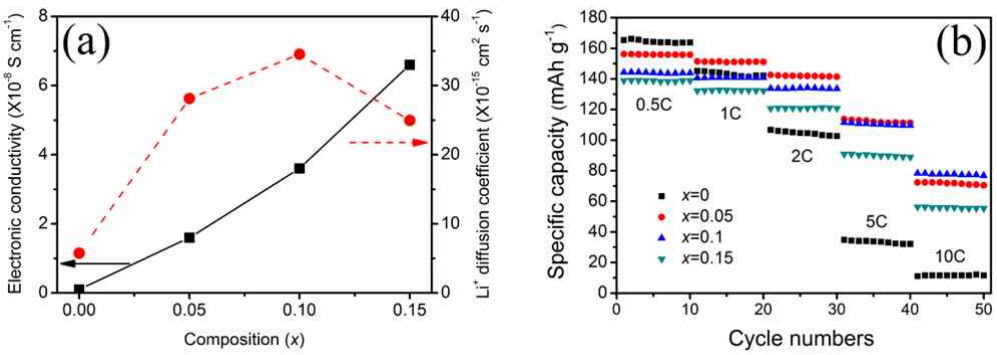

Figure 2. (a) Variation in electronic conductivity and Li^+ ion diffusion coefficient as a function of composition x in $Li_{4-2x}Cu_{3x}Ti_{5-x}O_{12}$ ($0 \leq x \leq 0.15$). (b) Rate performance of $Li_{4-2x}Cu_{3x}Ti_{5-x}O_{12}$ ($0 \leq x \leq 0.15$) samples at different rates: the first 10 cycles at 0.5 C, second at 1 C, third at 2 C and fourth at 5 C (identical discharge/charge rates were used).

method [28]. The substitution of Cl^- ions for O^{2-} ions not only increased the electronic conductivity in LTO particles through the generation of mixing Ti^{4+}/Ti^{3+}, but also enhanced the Li^+ ion diffusion coefficient in the particles. As a result, $Li_4Ti_5O_{11.8}Cl_{0.2}$ exhibited improved rate performance with a reversible capacity of 121 mAh g^{-1} at 2 C in 1.0～3.0 V, while that of the pristine LTO is only 90 mAh g^{-1}. Similarly, Qi et al. prepared $Li_4Ti_5O_{12-x}Br_x$ ($0 \leq x \leq 0.3$) through a high-temperature solid-state reaction method [29]. Both the electronic conductivity and the Li^+ ion diffusion coefficient in the particles were improved due to Br^- doping. Consequently, the optimized sample, $Li_4Ti_5O_{11.8}Br_{0.2}$, showed outstanding rate performance with a reversible capacity of 115 mAh g^{-1} at 10 C in 1.0～2.5 V, while that of the pristine LTO was only 45 mAh g^{-1}.

III. Compositing Strategy

In contrast to the doping strategy, compositing with a second conductive phase can distinctly improve the electrical conduction between LTO particles whereas it cannot alter the intrinsic conductivity (electronic conductivity and Li^+ ion diffusion coefficient) of LTO. The useful second conductive phase can be carbon, TiN, Cu, or Ag [30-44].

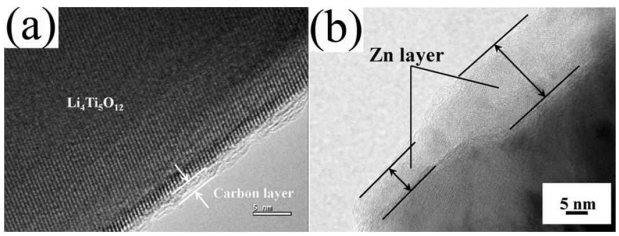

Figure 3. TEM images of LTO materials with (a) carbon coating [30] (Reprinted from Journal of Power Sources, Vol. 214, X.F. Guo, C.Y. Wang, M.M. Chen, J.Z. Wang, J.M. Zheng, Carbon coating of $Li_4Ti_5O_{12}$ using an amphiphilic carbonaceous material for improvement of lithium-ion battery performance, pp. 107～112. Copyright 2012, with permission from Elsevier.) and (b) Zn coating [41] (Reprinted from Journal of Alloys and Compounds, Vol. 513, C.T. Hsieh, B.S. Chang, J.Y. Lin, R.S. Juang, Improvement of rate capability of spinel lithium titanate anodes using microwave-assisted zinc nano-coating, pp. 393～398. Copyright 2012, with permission from Elsevier).

1. Compositing with carbon-based materials

Guo et al. synthesized carbon coated LTO through a hydrothermal method using an amphiphilic carbonaceous material as the carbon source [30]. The carbon existed as a uniform coating on the surface of the LTO particles, as presented in Fig. 3(a). The carbon coating improved the electrical conductivity between the LTO particles, leading to excellent rate performance of the carbon coated LTO material. At 20 C, this material delivered a high capacity of 137 mAh g^{-1} in 1.0～3.0 V. Wang et al. fabricated LTO/C composite anode materials through a simple starch sol assisted method using anatase TiO_2 and Li_2CO_3 as raw materials and soluble starch as a carbon source [31]. Due to the enhancement of electrical conduction between the particles, the optimized sample presented outstanding rate performance with a discharge capacity of 142 mAh g^{-1} at 5 C in 1.0～2.5 V. Yang et al. prepared a LTO/C composite through a facile solid-state reaction using Super-P-Li conductive carbon black as a reaction precursor in an Ar/H_2 atmosphere [32]. The conductive carbon was embedded in the LTO particles, enhancing the electrical conduction between the particles. As a result, the LTO/C exhibited improved rate performance with a capacity of 169 mAh g^{-1} at 1 C in 1.0～2.0 V. Li et al. fabricated nitrogen-doped carbon coated LTO using a pro-coating method combined with ball milling [33]. The uniformly coated nitrogen-doped carbon enhanced the electric conductivity between the particles, thereby resulting in excellent rate performance of LTO. The nitrogen-doped carbon coated LTO had a large ca-

pacity of 128 mAh g^{-1} at 20 C in 1.0～2.5 V. Zhang et al. prepared a N-doped carbon coated LTO composite using sugar as a carbon source and NH_3 as a nitrogen source [34]. The thickness of the carbon coatings was about 1～3 nm. Due to the N-doped carbon coating with high electrical conductivity, the composite showed outstanding rate performance. At 24 C, it delivered a large discharge capacity of 100 mAh g^{-1} in 1.0～3.0 V.

Wu et al. prepared LTO/carbon nanofibers composite through *in situ* growth of carbon fibers using a chemical vapor deposition method in a N_2/C_2H_2 atmosphere [35]. The deposited carbon fibers provided an efficient electrical conductive network. As a result, the composite exhibited excellent rate performance. It showed a large capacity of over 140 mAh g^{-1} at 10 C in 1.0～3.0 V. Fang et al. synthesized an LTO/acetylene black/multi-wall carbon nanotubes composite through a simple solid-state reaction method [36]. The electrical conductivity of the composite was improved by embedding LTO particles into the conductive acetylene black/multi-wall carbon nanotube network. Consequently, the composite presented outstanding rate performance with a reversible capacity of 116 mAh g^{-1} at 20 C and 102 mAh g^{-1} at 30 C in 1.0～3.0 V. Li et al. prepared a LTO/graphitized carbon nanotube composite through a solid-state reaction method in Ar atmosphere [37]. The valid graphitized carbon nanotube conductive network provided good contact between the LTO particles and thus benefited electronic transfer an the composite consequently showed good rate performance. At 10 C, its initial discharge capacity was 143 mAh g^{-1} in 1.0～3.0 V. Li et al. also fabricated an LTO/carbon/carbon nanotube composite through the same solid-state reaction method [38]. Compared with carbon or carbon nanotubes, the combination of carbon and carbon nanotubes provides more efficient electrical conductive networks. The results revealed that the composite exhibited outstanding rate performance with a discharge capacity of 148 mAh g^{-1} at 5 C and 143 mAh g^{-1} at 10 C in 1.0～3.0 V. Xiang et al. synthesized an LTO/graphene composite through a simple sol-gel method [39]. The carbon content was about 7.8 wt%. The LTO/graphene composite presented advanced rate performance. At 10 C, the composite had a reversible capacity of 146 mAh g^{-1} in 1.0～2.5 V. Yu et al. prepared an LTO/polyacene composite through *in situ* carbonization of phenol-formaldehyde resin route to form a carbon-based composite [40]. Polyacene was uniformly dispersed between the LTO particles, which improved the electrical contact between these particles. Consequently, this composite showed outstanding rate performance with a capacity of 136 mAh g^{-1} at 10 C in 1.0～2.0 V.

2. Compositing with non-carbon-based materials

Hsieh et al. synthesized Zn coated LTO through a microwave-assisted method [41]. Microwave heating rapidly deposited Zn layers over the surface of the LTO particles [see Fig. 3(b)]. The well-dispersed Zn layers offered electronic pathways over the LTO particles. This composite consequently exhibited high capacity retention of 78.1% at 10 C/0.2 C. Huang et al. prepared an LTO/Ag composite through an electroless deposition method [42]. The Ag particles were highly dispersed and had size of ＜20 nm. The Ag particles played a positive role in enhancing the electrical contact between the LTO particles, thereby improving the rate performance of LTO. At 10 C, the composite delivered a large discharge capacity of 115 mAh g^{-1} in 0.5～2.3 V. Huang et al. also fabricated an LTO/Cu composite through the same electroless deposition method [43]. The content of Cu was determined as 1%. The conductivity of the LTO/Cu composite was almost two orders of magnitude higher than that of pristine LTO. Consequently, the composite showed advanced rate performance with a first discharge capacity of 80 mAh g^{-1} at 10 C in 0.5～2.3 V.

Zhang et al. synthesized LTO/TiN composites through high-energy ball-milling of a mixture of LTO and TiN [44]. TiN existed as an amorphous coating on the LTO particles, and thus significantly enhanced the electrical conductivity between the LTO particles. As a result, the optimized sample, LTO/TiN with 2 wt % TiN, presented advanced rate performance with a high capacity of 130 mAh g^{-1} at 20 C in 1.0～3.0 V.

IV. Nanostructuring Strategy

Another strategy to improve the rate performance is to nanosize LTO. In this strategy, the electronic conductivity and Li^+ ion diffusion coefficient as well as the electrical conduction between LTO particles are essentially unchanged. Rather the improvement is due to the small particle size shortening electron and Li^+ ion transportation pathways within LTO particles. Various nanomaterials, including zero-dimensional [45-47], one-dimensional [48,49], two-dimensional [50], and three-dimensional [51-58] LTO materials, have been prepared.

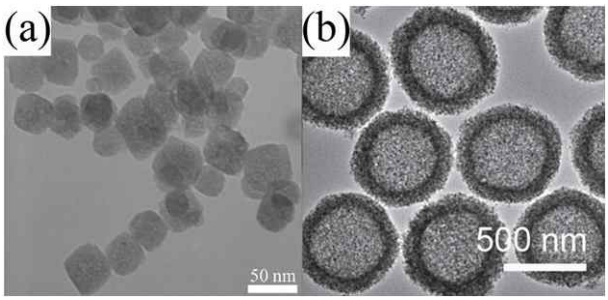

Figure 4. TEM images of LTO materials with (a) nanoparticle [45] (Reprinted from Journal of Power Sources, Vol. 202, J. Lu, C.Y. Nan, Q. Peng, Y.D. Li, Single crystalline lithium titanate nanostructure with enhanced rate performance for lithium ion battery, pp. 246～252. Copyright 2012, with permission from Elsevier), and (b) hollow sphere morphologies [51] (Reprinted from Advanced Materials, Vol. 25, L. Yu, H.B. Wu, X.W. Lou, Mesoporous $Li_4Ti_5O_{12}$ Hollow Spheres with Enhanced Lithium Storage Capability, pp. 2296～2300. Copyright 2013, with permission from WILEY-VCH Verlag GmbH & Co.).

1. Zero-dimensional LTO

Lu et al. prepared 40 nm near-uniform LTO single crystals through a hydrothermal method using cubic NaCl-type $(Li_{0.4}H_{0.6})_2TiO_3$ nanocrystals as the precursor, as shown in Fig. 4(a) [45]. The as-prepared LTO nanocrystals presented favorable rate performance: a reversible capacity of 140 mAh g^{-1} at 5 C in 0.9～2.5 V. Wu et al. synthesized LTO nanoparticles through a high-temperature solid-state reaction by adding prepared cellulose to an aqueous dispersion of TiO_2 and $LiAc{\cdot}H_2O$ [46]. These nanoparticles had an average particle size of 20～30 nm, and thus exhibited excellent rate performance. At 10 C, they delivered a large reversible capacity of 131 mAh g^{-1} in 1.0～3.0 V. Liu et al. fabricated LTO nanoparticles through a simple microemulsion method [47]. These nanoparticles were around 30～50 nm in size and had high crystallinity, and thereby displayed excellent rate performance with a large capacity of 130 mAh g^{-1} at 10 C in 0.8～2.5 V.

2. One-dimensional LTO

Jo et al. fabricated LTO nanofibers through an electrospinning method [48]. The diameter of these nanofibers could be controlled to be 200～600 nm. The nanofiber type of architecture could shorten the electron and Li^+ ion transport distance, leading to high rate performance. At 10 C, they delivered a large capacity of 138 mAh g^{-1} in 1.0～3.0 V. Wang et al. synthesized porous LTO fibers through the same electrospinning method [49]. These fibers had an average diameter of 230 nm and were composed of nanoparticles with an average diameter of 47.5 nm. The fibers showed excellent rate performance with a reversible capacity of 120 mAh g^{-1} at 10 C in 1.0～2.0 V.

3. Two-dimensional LTO

Hong et al. synthesized ultrathin LTO nanosheets through a hydrothermal route using ultrathin titanate nanowires as a precursor [50]. The synthesized LTO nanosheets have a large surface area of 159.2 $m^2 g^{-1}$ and their thickness was found to be 5～7 nm. These nanosheets consequently exhibited excellent rate performance. At a current density of 1 A g^{-1}, they delivered a large reversible capacity of 150 mAh g^{-1} in 1.0～2.5 V.

4. Three-dimensional LTO

Yu et al. synthesized mesoporous LTO hollow spheres with high quality through a templating approach [Fig. 4(b)] [51]. These spheres had mesoporous shells with tunable thickness. Benefiting from the unique structural features, these spheres exhibited advanced rate performance with a reversible capacity of 115 mAh g^{-1} at 10 C in 1.0～3.0 V. Chen et al. synthesized LTO microspheres assembled from sawtooth-like nanosheets through a hydrothermal process and subsequent thermal treatment [52]. The microspheres had diameters ranging from 400 to 600 nm, and a large specific surface area of 139.4 $m^2 g^{-1}$. As a result, the LTO microspheres exhibited high rate performance with a reversible capacity of 135 mAh g^{-1} at 57 C in 1.0～2.5 V. Yu et al. fabricated LTO nanostructured spherical particles through a one-pot template-free solvothermal method [53]. The as-synthesized particles had sizes of 1～2 μm, and were constructed by LTO nanocrystallites in a size range of a few nanometers. Consequently, these particles showed advanced rate performance with a reversible capacity of about 85 mAh g^{-1} at 30 C in 1.0～2.5 V. He et al. prepared monodispersed LTO hollow spheres using carbon spheres as a template [54]. The LTO hollow spheres had an average outer diameter of 1.0 μm and an average wall thickness of 60 nm. As a result, they exhibited favorable rate performance with a specific capacity of 100 mAh g^{-1} at 10 C in 1.0～3.0 V. Chou et al. synthesized LTO microspheres through a combination of a microwave-assisted hydrothermal method and a microwave post-annealing process [55]. The as-prepared LTO microspheres had sizes of 500～800 nm, and were composed of small nanoflakes of around 10 nm thickness, leading to advanced rate performance. At 20 C, this material delivered a specific capacity of about 100 mAh g^{-1} in 1.0～3.0 V using carboxymethyl cellulose as a binder. Shao et al. prepared nanoporous LTO through a sol-gel method using monodispersed polystyrene spheres as a template [56]. The nanoporous structure had an average diameter of approximately 100 nm and a wall thickness of about 50 nm. As a result, this nanoporous LTO material showed advanced rate performance with a specific capacity of 102 mAh g^{-1} at 10 C in 0.5～3.0 V. Lin et al. fabricated mesoporous LTO spheres under a hydrothermal environment and calcinations [57]. Acidized carbon black was introduced into the fabrication. The pore size in the mesoprous LTO spheres was about 4 nm. These spheres displayed good rate performance. Their reversible capacity at 30 C remained over half of that at 0.5 C. Huang et al. prepared a hollow spherical LTO material through a macroemulsion method [58]. The hollow spheres had a diameter of around 1 μm, and their walls were constructed by a large number of nanoparticles of around 100 nm diameter. Consequently, this material exhibited excellent rate performance. At 20 C, it had a stable capacity of 115 mAh g^{-1} in 1.0～3.0 V.

V. Conclusions

A doping strategy can be adopted to improve the electronic conductivity and/or Li^+ ion diffusion coefficient in LTO particles, and thereupon the rate performance of LTO. Doping can tailor structural ar-

rangements, thus altering the Li^+ ion diffusion coefficient. Moreover, doping can introduce conductive ions and thus improve electronic conductivity. Although many doping strategies have improved the rate performance, three limitations exist with this approach. First, doping cannot enhance the electrical conduction between particles. As a result, the rate performance cannot be significantly improved. Second, existing studies of material composition, material structure, material properties, and LIB performances are unsatisfactory. The role of the material structure is still not clear. It is well known that material structure significantly determines material properties and ultimately LIB performance. Thus, it is imperative to investigate doping strategies based on an intensive study of material structure. Finally, studies on existing doping techniques are not sufficient given that a law for doping of LTO has not been unveiled. It is therefore necessary to systematically investigate doped LTO and to reveal the law.

Another way to improve the rate performance is to incorporate a conductive second phase. Despite a simple and cost effective process, the compositing strategy can only improve the electrical conduction between the particles but cannot modify the intrinsic conductivity of LTO. Its capability for improving the rate performance is therefore limited.

Synthesizing nanosized LTO is an effective way to improve the rate performance. In general, nanosized LTO materials can have good rate performance due to reduced particle size, which can shorten the distance of electron conduction and Li^+ ion transport within particles. However, the intrinsic and extrinsic conductivities are essentially unchanged in this strategy. Moreover, nanosized LTO materials generally suffer from low initial coulombic efficiency and poor cyclic stability due to their relatively lower crystallinity. In addition, nanosized LTO materials, excluding mesoporous LTO spheres, have the common problem of low tap density.

Based on the above analysis, it is clear that none of the three strategies can simultaneously improve the intrinsic and extrinsic conductivities of LTO and reduce the particle size. These properties, however, may be simultaneously improved through synergistic strategies combining doping, compositing, and nanostructuring. Therefore, the following research directions in the field of LTO could be pursued: i) developing synergistic strategies to effectively improve the performance of LTO, and ii) investigating the relations among the material composition, material structure, material properties, and LIB performances in order to unveil a law for the doping of LTO.

Acknowledgements

This research was supported by the Agency for Science, Technology and Research, Singapore through the Singapore-China Joint Research Programme (R265-000-442-305 and No.2012DFG52130).

References

[1] M. Armand and J. M. Tarascon, Nature **451,** 652 (2008).
[2] M. Yoshio, H. Y. Wang, K. Fukuda, Y. Hara, and Y. Adachi, J. Electrochem. Soc. **147,** 1245 (2000).
[3] S. S. Zhang, K. Xu, and T. R. Jow, J. Power Sources **160,** 1349 (2006).
[4] S. S. Zheng, J. Power Sources **161,** 1385 (2006).
[5] A. D. Robertson, L. Trevino, H. Tukamoto, and J. T. S. Irvine, J. Power Sources **81,** 352 (1999).
[6] K. M. Colbow, J. R. Dahn, and R. R. Haering, J. Power Sources **26,** 397 (1989).
[7] J. B. Goodenough, and Y. Kim, Chem. Mater. **22,** 587 (2010).
[8] T. Ohzuku, A. Ueda, and N. Yamamoto, J. Electrochem. Soc. **142,** 1431 (1995).

[9] C. H. Chen, J. T. Vaughey, A. N. Jansen, D. W. Dees, A. J. Kahaian, T. Goacher, and M. M. Thackeray, J. Electrochem. Soc. **148,** A102 (2001).

[10] T. F. Yi, Y. Xie, Q. J. Wu, H. P. Liu, L. J. Jiang, M. F. Ye, and R. S. Zhu, J. Power Sources **214,** 220 (2012).

[11] Q. Y. Zhang, C. L. Zhang, B. Li, S. F. Kang, X. Li, and Y. G. Wang, Electrochim. Acta **98,** 146 (2013) .

[12] C. H. Chen, J. T. Vaughey, A. N. Jansen, D. W. Dees, A. J. Kahaian, T. Goacher, and M. M. Thackeray, J. Electrochem. Soc. **148,** A102 (2001).

[13] H. L. Zhao, Y. Li, Z. M. Zhu, J. Lin, Z. H. Tian, and R. L. Wang, Electrochim. Acta **53,** 7079 (2008).

[14] J. Y. Lin, C. C. Hsu, H. P. Ho, and S. H. Wu, Electrochim. Acta **87,** 126 (2013).

[15] X. L. Zhang, G. R. Hu, Z. D. Peng, and J. Inorg. Mater. **26,** 443 (2011).

[16] B. B. Tian, H. F. Xiang, L. Zhang, H. H. Wang, J. Solid State Electrochem. **16,** 205 (2012).

[17] B. B. Tian, H. F. Xiang, L. Zhang, Z. Li, H. H. Wang, Electrochim. Acta **55,** 5453 (2010).

[18] T. F. Yi, H. P. Liu, Y. R. Zhu, L. J. Jiang, Y. Xie, and R. S. Zhu, J. Power Sources **215,** 258 (2012).

[19] W. Wang, H. L. Wang, S. B. Wang, Y. J. Hu, Q. X. Tian, and S. Q. Jiao, J. Power Sources **228,** 244 (2013).

[20] T. F. Yi, B. Chen, H. Y. Shen, R .S. Zhu, A. N. Zhou, and H. B. Qiao, J. Alloy Compd. **558,** 11 (2013).

[21] X. L. Zhang, G. R. Hu, and Z. D. Peng, J. Cent. South Univ. **20,** 1151 (2013).

[22] T. F. Yi, Y. Xie, Q. J. Wu, H. P. Liu, L. J. Jiang, M. F. Ye, and R. S. Zhu, J. Power Sources **214,** 220 (2012).

[23] Z. J. Yu, X. F. Zhang, G. L. Yang, J. Liu, J. W. Wang, R. S. Wang, and J. P. Zhang, Electrochim. Acta **56,** 8611 (2011).

[24] G. R. Hu, X. L. Zhang, and Z. D. Peng, Trans. Nonferrous Met. Soc. China **21,** 2248 (2011).

[25] Y. K. Sun, D. J. Jung, Y. S. Lee, and K. S. Nahm, J. Power Sources **125,** 242 (2004).

[26] C. F. Lin, M. O. Lai, L. Lu, H. H. Zhou, and Y. L. Xin, J. Power Sources **244,** 272 (2013).

[27] C. F. Lin, B. Ding, Y. L. Xin, F. Q. Cheng, M. O. Lai, L. Lu, and H. H. Zhou, J. Power Sources **248,** 1034 (2014).

[28] Y. D. Huang, Y. L. Qi, D. Z. Jia, X. C. Wang, Z. P. Guo, and W. I. Cho, J. Solid State Electrochem. **16,** 2011 (2012).

[29] Y. L. Qi, Y. D. Huang, D. Z. Jia, S. J. Bao, and Z. P. Guo, Electrochim. Acta **54,** 4772 (2009).

[30] X. F. Guo, C. Y. Wang, M. M. Chen, J. Z. Wang, and J. M. Zheng, J. Power Sources **214,** 107 (2012).

[31] L. Wang, Z. L. Zhang, G. C. Liang, X. Q. Ou, and Y. Q. Xu, Power Technol. **215,** 79 (2012).

[32] L. X. Yang and L. J. Gao, J. Alloy Compd. **485,** 93 (2009).

[33] H. S. Li, L. F. Shen, X. G. Zhang, J. Wang, P. Nie, Q. Che, and B. Ding, J. Power Sources **221,** 122 (2013).

[34] H. Q. Zhang, Q. J. Deng, C. X. Mou, Z. L. Huang, Y. Wang, A. J. Zhou, and J. Z. Li, J. Power Sources **239,** 538 (2013).

[35] C. Y. Wu, Y. X. Wang, J. Xie, G. S. Cao, T. J. Zhu, and X. B. Zhao, J. Electrochem. Soc. **16,** 3915 (2012).

[36] W. Fang, P. J. Zuo, Y. L. Ma, X. Q. Cheng, L. X. Liao, and G. P. Yin, Electrochim. Acta **94,** 294 (2013).

[37] X. Li, M. Z. Qu, and Z. L. Yu, Solid State Ionics **181,** 635 (2010).

[38] X. Li, M. Z. Qu, Y. J. Huai, and Z. L. Yu, Electrochim. Acta **55,** 2978 (2010).

[39] H. F. Xiang, B. B. Tian, P. C. Lian, Z. Li, and H. H. Wang, J. Alloy Compd. **509,** 7205 (2011).

[40] H. Y. Yu, X. F. Zhang, A. F. Jalbout, X. D. Yan, X. M. Pan, H. M. Xie, and R. S. Wang, Electrochim. Acta **53,** 4200 (2008).

[41] C. T. Hsieh, B. S. Chang, J. Y. Lin, and R. S. Juang, J. Alloy Compd. **513,** 393 (2012).

[42] S. H. Huang, Z. Y. Wen, J. C. Zhang, and X. L. Yang, Electrochim. Acta **52,** 3704 (2007).

[43] S. H. Huang, Z. Y. Wen, B. Lin, J. D. Han, and X. G. Xu, J. Alloy Compd. **457,** 400 (2008).

[44] J. W. Zhang, J. W. Zhang, W. Cai, F. L. Zhang, L. G. Yu, Z. S. Wu, and Z. J. Zhang, J. Power Sources **211,** 133 (2012).

[45] J. Lu, C. Y. Nan, Q. Peng, and Y. D. Li, J. Power Sources **202,** 246 (2012).

[46] H. L. Wu, Y. D. Huang, D. Z. Jia, Z. P. Guo, and M. Miao, J. Nanopart. Res. **14,** 713 (2012).

[47] G. Y. Liu, H. Y. Wang, G. Q. Liu, Z. Z. Yang, B. Jin, and Q. C. Jiang, J. Power Sources **220,** 84 (2012).

[48] M. R. Jo, Y. S. Jung, and Y. M. Kang, Nanoscale **4,** 6870 (2012).

[49] L. Wang, Q. Z. Xiao, Z. H. Li, G. T. Lei, P. Zhang, and L. J. Wu, J. Solid State Electrochem. **16,** 3307 (2012).

[50] Z. S. Hong, T. B. Lan, H. X. Zhang, L. L. Jiang, and M. D. Wei, Funct. Mater. Lett. **4,** 389 (2011).

[51] L. Yu, H. B. Wu, and X. W. Lou, Adv. Mater. **25,** 2296 (2013).

[52] J. Z. Chen, L. Yang, S. H. Fang, and Y. F. Tang, Electrochim. Acta **55,** 6596 (2010).

[53] S. H. Yu, A. Pucci, T. Herntrich, M. G. Willinger, S. H. Baek, Y. E. Sung, and N. Pinna, J. Mater. Chem. **21,** 806 (2011).

[54] N. D. He, B .S. Wang, and J. J. Huang, J. Solid State Electrochem. **14,** 1241 (2010).

[55] S. L. Chou, J. Z. Wang, H. K. Liu, and S. X. Dou, J. Phys. Chem. C **115,** 16220 (2011).

[56] D. Shao, J. R. He, Y. Luo, W. Liu, X. Y. Yu, and Y. P. Fang, J. Solid State Electrochem. **16,** 2047 (2012).

[57] Y. S. Lin and J. G. Duh, J. Power Sources **196,** 10698 (2011).

[58] J. J. Huang and Z. Y. Jiang, Electrochem. Solid-State Lett. **11,** A116 (2008).